Time-scales for Non-Inductive Current Buildup In Low-Aspect-Ratio Toroidal Geometry

S. C. Jardin

Princeton Plasma Physics Laboratory
Princeton University
Princeton, NJ 08543

November 1999

Abstract

The fundamental differences between inductive and non-inductive current buildup are clarified and the associated time-scales and other implications are discussed. A simulation is presented whereby the plasma current in a low-aspect-ratio torus is increased primarily by the self-generated bootstrap current with only 10% coming from external current drive. The maximum obtainable plasma current by this process is shown to scale with the toroidal field strength. The basic physics setting the time-scales can be obtained from a 1D analysis. Comparisons are made between the timescales found here and those reported in the experimental literature.

I. Introduction

There is considerable interest in using non-inductive current drive to establish, maintain, control, and modify the current distribution in low-aspect-ratio toroidal fusion experiments, often called spherical tori, spherical tokamaks, or STs [1]. This interest stems from the fundamental geometry of a low-aspect-ratio torus, which precludes the presence of a large internal solenoid or "OH" coil. While present laboratory experiments [2-5] are equipped with relatively small OH coils for inductive current buildup, it is expected that the next generation of experiments and reactor concepts will rely totally on non-inductive techniques [6] .

The non-inductive sources of current drive under consideration could be due to RF, bootstrap current, and/or neutral beams [7]. In this paper we clarify the fundamental differences between inductive and non-inductive current buildup, discuss the associated time-scales, and illuminate some of the consequences of attempting to exceed these natural time-scales. We explicitly do *not* consider non-axisymmetric current drive techniques such as coaxial helicity injection (CHI) [8] in the present paper.

The essential physics describing both inductive and non-inductive current rampup is contained within the TSC code [9,10]. Surface average equations are solved for the evolution of the magnetic transform and plasma energy, with external sources of energy and current, and with realistic magnetic boundary conditions coupled to the changing currents in the poloidal field coils. For definiteness, this is applied to the geometry and parameters of a possible future upgrade to the National Spherical Torus Experiment (NSTX) [5].

Inductive and non-inductive techniques for plasma current buildup are fundamentally different. In the MHD description, inductive current drive takes the form of a changing boundary condition in the magnetic field evolution equation whereas non-inductive current drive takes the form of a source term in that equation. This difference can lead to the formation of large transient effects in the current profile for the non-inductive case unless the source terms are turned on slowly compared to the natural time scale.

An associated and compounding effect is that inductive current drive changes the plasma flux most near the plasma boundary, where the temperature is lowest, whereas non-inductive current drive must change the plasma flux most near the plasma magnetic axis, where the temperature is greatest. This difference makes the natural time scale even longer for the non-inductive current drive.

The role of the external poloidal field coils (which produce the vertical field needed for equilibrium) in providing volt-seconds for the non-inductive current rampup is clarified. These coils provide an essential field needed for equilibrium, but a simple graphical argument shows that these can never produce all of the flux change needed for current buildup.

We describe simulations performed with the TSC code showing that it should be possible to ramp up the plasma current in NSTX using non-inductive current drive. The time scales for this depend on the plasma temperature, but also depend on the fraction of bootstrap current during the rampup. For typical central plasma temperatures of 3-5 keV, the natural current rampup timescale for high bootstrap fraction (over 50%) rampup would be several tens of seconds. Attempts to exceed this natural timescale can lead to distorted and unstable current profiles. In extreme cases of sudden application of a current drive profile typical of a high bootstrap fraction plasma, the central plasma current can actually be driven negative, resulting in certain instability.

Very high bootstrap fraction plasmas (f_{BS} > 90%) must operate at high values of poloidal beta, $\beta_P \cong 2$. The effect of MHD stability constraints is to make the maximum allowable plasma current for these plasmas proportional to the toroidal field strength. Increasing the maximum toroidal field capability in NSTX is shown to increase the maximum value of plasma current obtainable through bootstrap overdrive, while maintaining MHD stability.

General scaling relations are derived and a physical picture is given. A simple "1D" model that contains the essential physics can predict the plasma trajectory in (l_i,q) space during the rampup. The scaling relations are seen to agree with the detailed 2D TSC simulations of non-inductive current rise in NSTX and to be consistent with existing experiments.

II. Inductive vs. Non-Inductive Current Buildup

Here we compare two different methods for increasing the toroidal current in a low aspect ratio (spherical) tokamak (or ST), *inductive* and *non-inductive*. It is instructive to consider the time evolution of the midplane poloidal magnetic flux for these two cases. We work in the normal (R,φ,Z) cylindrical coordinate system for axisymmetric systems shown in Fig. 1 whereby φ is the symmetry angle, R is the major radius, and Z is the vertical (or axial) direction. For simplicity, we consider an up/down symmetric configuration where the magnetic axis lies on the midplane, Z=0. The midplane poloidal magnetic flux is defined as the integral of the Z component of the total magnetic field, B_Z(R,Z) times the area in a disk centered at the symmetry axis and lying in the $Z=0$ plane, extending out to the radius R. The midplane poloidal magnetic flux is thus defined by the integral,

$$\Psi(R,0) = -\iint_{disk} \vec{B} \bullet d\vec{A} = -2\pi \int_0^R B_Z(R,0) R dR \tag{1}$$

This definition is consistent with the normal representation for the magnetic field in an axisymmetric system [11]

$$\vec{B} = \frac{1}{2\pi} \nabla\varphi \times \nabla\Psi + (R^2 \vec{B} \bullet \nabla\varphi)\nabla\varphi. \tag{2}$$

Note that the arbitrary constant in Ψ when defined by Eq. (2) is determined by the definition in Eq. (1) so that $\Psi(0,Z) = 0$.

It is also useful to define an internal inductance L_i as the ratio of the internal poloidal magnetic flux (i.e. the difference between the poloidal magnetic flux at the plasma limiter and at the magnetic axis) to the total plasma current [12], thus

$$L_i = \frac{\Psi_{limiter} - \Psi_{axis}}{I_P} \equiv \frac{\Delta\Psi}{I_P} = \frac{\iiint_{plasma} \vec{B} \bullet \nabla\theta \, dV}{\iiint_{plasma} \vec{J} \bullet \nabla\varphi \, dV} \tag{3}$$

Here θ and φ are the poloidal and toroidal angles as shown in Fig. 1 and the integrals of the magnetic field and current density are over the plasma volume inside the contour $\Psi=\Psi_{\text{limiter}}$. Clearly, L_i depends on the plasma toroidal current profile. In the discussion that follows, we assume that L_i is relatively constant in time so that an increase in plasma current corresponds to a proportional increase in internal poloidal magnetic flux.

The poloidal flux at the magnetic axis evolves according to the well-known equation [7]

$$\frac{\partial \Psi_{axis}}{\partial t} = 2\pi\eta_0 R^2 (\vec{J} - \vec{J}_{CD}) \bullet \nabla\varphi \tag{4}$$

Here η_0 is the resistivity at the magnetic axis, R is the major radius,

$$R\,\vec{J} \bullet \nabla\varphi = \frac{1}{2\pi\mu_0 R}\Delta^*\Psi = \frac{R}{2\pi\mu_0}\nabla \bullet R^{-2}\nabla\Psi \tag{5}$$

is the toroidal current density (mks units), and J_{CD} is the non-inductive current drive term, all evaluated at the magnetic axis.

We illustrate in Figs. 2(a) and 2(b) typical computed sequences of the midplane poloidal magnetic flux for two methods of increasing the plasma toroidal current in a ST. In particular, we consider inductive 2(a) and non-inductive 2(b) current buildup sequences using the geometry of NSTX .

Figure 2(a) illustrates inductive current buildup, which is the standard method of increasing the current in a toroidal device. It uses an external transformer, or OH transformer, which is a solonoidal stack of coils in the interior of the plasma torus as shown in Fig. 1. The first curve in the sequence in Fig. 2(a) corresponds to an initial plasma toroidal current of 100 kA, with the transformer initially carrying a toroidal current in the same direction as the plasma toroidal current. The two limiter points where the plasma-vacuum interface crosses the $Z=0$ plane are marked with solid dots, and the horizontal line connecting them corresponds to the value of the poloidal magnetic flux at the limiter at that time, $\Psi_{limiter}$. The minimum in the curve between those two points corresponds to the magnetic axis, $\Psi=\Psi_{axis}$, marked with open triangles.

To increase the plasma current, the OH transformer current is decreased in magnitude to increase the poloidal flux at the inside edge of the plasma, $\Psi_{limiter}$. Since there is no non-inductive current drive in this case, $J_{CD} = 0$ in Eq. (4) and Ψ_{axis} will also increase monotonically in time as given by Eq. (4), but at a slow rate determined by the axis value of the plasma resistivity. If $\Psi_{limiter}$ is made to increase faster than Ψ_{axis} , and if it is accompanied by an adjustment in the external equilibrium fields so that the poloidal flux at the outside edge increases at the same rate, then the poloidal flux difference between the magnetic axis and the limiter will increase in time as shown in Fig. 2(a). This corresponds to an inductive increase in the plasma current.

We can make a simple estimate of how much the poloidal flux at the limiter changes as a result of a change in the currents in those coils. If the OH coils are a solonoidal stack of coils of height d (i.e., $\mp d/2$) and radius R_{OH} as shown in Fig. 1, and if $R_{OH} << d,$ then the increase in poloidal flux at the inside plasma limiter when the current in the OH solenoid changes by ΔI_{OH} is given by (mks units)

$$\Delta\Psi_{\mathrm{lim}iter} = -\pi\mu_0 R_{OH}^2 \Delta I_{OH} / d \tag{6}$$

As mentioned above, the currents in the outer poloidal field coils must also change as the plasma current increases to keep the plasma in equilibrium with the desired shape. However, it is clear from Eq. (6) that a changing current in the OH coils is absolutely necessary in order to increase the poloidal flux at the limiter. In other words, *a low-aspect-ratio tokamak cannot be operated inductively without an OH coil*. Although obvious from the picture presented here, there has been confusion on this point previously where some have incorrectly predicted that the outer poloidal field coils by themselves could provide enough flux to ramp up the plasma current in a high beta ST. The only way that this could happen is if it was accompanied by a large geometry and/or inductance change so that the same plasma poloidal flux corresponded to a larger current

Next, consider the situation illustrated in Fig. 2(b) of a non-inductive buildup of the plasma current. Here, there is no OH coil or coil current and thus the value of the poloidal flux at the limiter stays essentially unchanged, consistent with Eq. (6). In this non-inductive case, the poloidal flux difference and the current in the plasma are increased by *decreasing* the value of the poloidal flux at the magnetic axis and at other locations in the plasma. This is accomplished using current drive as described in Eq. (4) with $J_{CD} > 0$. It is clear from comparing Figs. 2(a) and 2(b) that these two processes for increasing the plasma poloidal flux $(\Psi_{limiter} - \Psi_{axis})$ and the associated plasma toroidal current are qualitatively different since the first relies on *increasing* $\Psi_{limiter}$ and the second on *decreasing* Ψ_{axis}.

Note that for the non-inductive current buildup calculation presented in Fig. 2(b), one would calculate that the outer poloidal field coils provided a positive flux increase of 0.35 Webers (or Volt-seconds) at (R,Z) = (0.80,0) as the plasma current increased from 100 kA to 750 kA. This field increase was essential to maintain the plasma in equilibrium, but it clearly was not responsible for building up the plasma poloidal flux, as this process required the flux at the magnetic axis to *decrease* not *increase*.

III. Non-Inductive Current Buildup in NSTX

We have used the Tokamak Simulation Code (TSC) to calculate the feasibility of non-inductive current buildup in NSTX. The details of the calculational model are given in Refs[9-10]. Here we present the results of an optimized calculation where the plasma current is increased primarily due to the self-generated plasma bootstrap current. As the plasma is heated at low current and the plasma pressure increases, the sum of the computed bootstrap current and the other non-inductive current sources applied exceeds the plasma current, and thus acts to increase that current. In this simulation, the bootstrap current provides over 90% of the current-drive needed to buildup the plasma current. The remaining 10% is provided by a model external current-drive profile typical of radio frequency (RFCD) or neutral beam current drive (NBCD):

$$J_{ECD} = J_{ECD}(t)\frac{\tilde{\psi}^a(1-\tilde{\psi}^b)d^2}{d^2+(\tilde{\psi}-\tilde{\psi}_0)^2}$$

In these calculations, $a=0$, $b=1$, $d=0.2$, $\psi_0=0$, and $J_{ECD}(t)$ is determined so the total integrated current is I_{ECD} shown in Table I.

Table I: Results of TSC simulation of high bootstrap current rampup in NSTX-U

time	% β	T_{e0}	n_0	β_θ	$\ell i/2$	C_T	B_T	I_P	I_{ECD}	I_{BS}
0	0.1	140	1.10	1.0	.707	.54	0.61	100	50	37
4	0.4	400	1.65	1.6	.274	1.0	0.61	113	60	61
8	0.8	550	2.20	1.7	.249	1.3	0.61	222	70	174
12	1.4	700	3.30	1.7	.237	1.7	0.61	310	70	242
16	1.8	1000	3.50	1.8	.238	2.1	0.61	334	70	272
20	2.3	1200	3.70	1.8	.266	2.6	0.61	350	70	280
27	2.3	1700	4.40	2.0	.257	2.9	0.71	399	70	337
38	3.2	2500	4.80	2.1	.238	3.1	0.80	536	70	497
52	3.4	3000	5.30	2.2	.241	3.1	0.89	615	70	578
62	3.3	3600	5.50	2.2	.239	3.2	0.99	674	70	622
72	3.5	4350	5.50	2.2	.233	3.2	1.05	747	70	700
140	3.7	4506	5.50	2.1	.264	3.4	1.05	736	70	665

The results of this calculation are given in Table 1 and in Figs. 3-6.
In Table I, time is in seconds, % β is the definition which uses the square of the vacuum toroidal field at R=0.85 m in the denominator, T_{e0} is central electron temperature in eV, $n_0 \times 10^{19}$ m^{-3} is central electron density, β_θ is poloidal beta, $\ell i/2$ is internal inductance, C_T is Troyon factor a B_T (%β)/I_P with units %-meter-Tesla/MA, B_T is vacuum toroidal field in Tesla at R=0.85 m, I_P, I_{ECD}, and I_{BS} are total plasma current, externally driven plasma current, and bootstrap current in kA.

The external coil currents were adjusted during the calculation to keep the plasma shape approximately constant at major radius R= 0.82 m , minor radius a = 0.62 m, ellipticity $\kappa = 2.0$ and triangularity $\delta = 0.36$. The plasma Z_{EFF} was taken to be equal to 2.0 throughout. The plasma density profile and time evolution were prescribed. The density profile was given in tern of the time dependent central value and normalized poloidal flux by

$$n(\tilde{\psi},t) = n_0(t)\left[0.9\left(1-\tilde{\psi}^6\right)^{1/2} + 0.1\right] \tag{7}$$

This corresponds to a peak to volume-average ratio of about 1.4. The temperature profiles were computed from a transport model as described in

[10], but came out to have peak to volume-averaged ratios of approximately 2.7 (electrons) and 2.45 (ions). The final ion temperature was $T_{i0} = 2079\ eV$. The injected power was ramped up to 15 MW (total) over the first 72 seconds and held steady after that. The final stored energy of 0.3 MJ corresponds to an energy confinement time of $\tau_E = 20$ msec.

Figure 3 shows the time-history of the key scalar parameters characterizing the plasma as a function of time during the evolution. The time evolution of the total plasma current is given in Fig. 3(a) as well as the computed contributions due to the bootstrap current and the other current drive source terms. The time-scale over which the evolution occurred is very close to the fastest allowable by the physics. Attempts to accelerate the plasma current evolution with these same bootstrap current fractions resulted in code failure due to the formation of extreme hollow current profiles and concomitant disappearance of the magnetic axis. This phenomenon is described more completely in the next section.

Note that the external sources of heat and density become constant in time at $t=72$ sec. Even though the current buildup had been very gradual over this time, it still requires another 40-45 sec for the profiles to reach their steady-state values. These times are to be compared with that obtained by simple dimensional evaluation of Eq. (4) with $T_{e0} = 4300\ eV,\ a = 0.65,\ ln\ \Lambda = 17,$ and $Z_{EFF}=2$, which gives a characteristic time of $t_0 = a^2\ \mu_0\ /\ \eta(0) = 85\ sec.$

The time development of the plasma pressure and toroidal current density are shown in Figs. 4 and 5, and the final contours and midplane values of the plasma poloidal flux and current density are shown in Fig. 6. These profiles have the distinctive shape of a high $\varepsilon\beta_P$ equilibrium. Note that for the profiles, aspect ratio, and bootstrap model used here, we find that a plasma bootstrap fraction of 90% corresponds to a poloidal beta value of approximately 2, i.e. $\beta_P \cong 2$. Since $I_P \propto a\ B_T\ C_T\ /\ \beta_P$, if the Troyon coefficient C_T is fixed by stability limits and if the geometry stays fixed, the maximum plasma current will scale with the toroidal field strength, $I_P \propto B_T$.

IV. A Simple Illustration in 1D

Here we consider a simple example in one dimension by making use of the large aspect ratio toroidal expansion, but keeping essential toroidal effects.

If we denote by $\psi(r,t)$ the usual cylindrical poloidal flux function, then in the presence of a strong toroidal magnetic field and of a non-inductive current drive source, we have the evolution equation:

$$\frac{\partial\psi}{\partial t} = \eta(r)\left[\frac{1}{\mu_0 r}\frac{\partial}{\partial r} r \frac{\partial\psi}{\partial r} - j_{CD}(r,t)\right] \tag{8}$$

with either the non-inductive boundary condition[13]

$$\psi + \frac{a}{R\mu_0} L_{ext}^{eff} \frac{\partial\psi}{\partial r} = 0 \tag{9}$$

or the inductive boundary condition

$$\frac{2\pi a}{\mu_0}\frac{\partial\psi}{\partial r} = I_P(t)\,. \tag{10}$$

In Eq. (9), we have defined the effective external inductance as

$$\begin{aligned} L_{ext}^{eff} &\cong \left[\mu_0 R \ln(\frac{8R}{a}) - 2\right] + VF \\ &\cong \frac{3}{4}\left[\mu_0 R \ln(\frac{8R}{a}) - 2\right] \end{aligned} \tag{11}$$

Where the contribution of the vertical field (*VF*) is used to reduce the effective plasma inductance. [13-14]

The resistivity function is taken to have the following form

$$\eta(r) = \eta_0 \left[0.9\,(1 - \frac{r^2}{a^2})^m + 0.1\right]^{-3/2} \tag{12}$$

with m=8/3 unless otherwise specified. The current-drive source, $j_{CD}(r,t)$ is of the form:

$$j_{CD}(r,t) = \frac{I_{CD}(t)}{\pi a^2}\left[(1 - f_{BS})(n+1)(1 - \frac{r^2}{a^2})^n + \frac{45}{16} f_{BS} (\frac{r}{a})^{1/2} (1 - \frac{r^2}{a^2})\right] \tag{13}$$

where the first term in the square bracket represents current drive due to centrally peaked RF or NBI source (with n=4 in these examples), and the second term represents current drive due to the bootstrap current. The total integrated current source is specified as a function of time, $I_{CD}(t)$, and the fraction of the total current due to the bootstrap current is f_{BS} . For the examples presented here, we prepare the plasma in an initial equilibrium satisfying

$$\frac{1}{\mu_0 r}\frac{\partial}{\partial r} r \frac{\partial \psi}{\partial r} = j_0 \eta^{-1}(r) \tag{14}$$

with the constant j_0 and the boundary value of ψ chosen so that both the total initial plasma current and the non-inductive boundary condition are satisfied.

Note that the evolution Eq. (7) for the cylindrical poloidal flux function ψ implies the following evolution equation for the toroidal current density $j(r,t)$:

$$\frac{\partial j}{\partial t} = \frac{1}{\mu_0 r}\frac{\partial}{\partial r} r \frac{\partial}{\partial r}\left[\eta(r) j\right] + S_{CD}(r,t) \tag{15}$$

with

$$S_{CD}(r,t) = -\frac{1}{\mu_0 r}\frac{\partial}{\partial r} r \frac{\partial}{\partial r}\left[\eta(r) j_{CD}(r,t)\right]. \tag{16}$$

The results of three companion calculations with the same initial conditions and the same target current trajectory are shown in Fig. 7. Note that for the figures, the time is normalized to the diffusion time based on the central value of the resistivity,

$$t_0 = a^2 \mu_0 / \eta(0). \tag{17}$$

In 7(a), the plasma current is inductively ramped up from $0.1\ I_0$ to I_0 in a time $t_1 = 0.1\ t_0$. In 7(b), the current source is ramped up linearly from $0.1\ I_0$ to I_0 in a time $t_1 = 0.1\ t_0$, with 50% bootstrap current so that $f_{BS}=0.5$. In 7(c), we repeat 7(b) but with $f_{BS}=0.90$ so that all the current drive current is of the form of the bootstrap current. In each of the three cases, besides plotting the total plasma current vs. time, we also plot the time history of the internal inductance, $l_i/2$, defined as:

$$l_i/2 \equiv \frac{1}{a^2\left(\frac{\partial\psi}{\partial r}\right)^2_{r=a}}\int_0^a r\left(\frac{\partial\psi}{\partial r}\right)^2 dr \tag{18}$$

In comparing cases 7(a), 7(b), and 7(c), we note two striking features. The first is that the time-scale for equilibration for the non-inductive current-drive cases 7(b) and 7(c) is about 5 times as long as it is for the inductive current rampup case 7(a), even though the requested current is being increased at the same rate. However, in the inductive case 7(a) it is being driven by a boundary condition, whereas in the non-inductive cases 7(b) and 7(c) it is being driven by a source term. The second feature to note is that the internal inductance changes very rapidly at early times for case 7(c), indicating that sudden application of a bootstrap current drive can induce large transients in the plasma current profile.

These features of non-inductive current drive are further illustrated in Figs. 8-10, which are mere tabulations of cases similar to those illustrated in Fig. 7, but with the parameters systematically changed. Figure 8 shows how the time at which it takes the plasma current to reach 99% of it's final value depends on the current turnon time t_1. For the inductive case 7(a), this time is the same as the turnon time, whereas for all the non-inductive current-drive cases it is significantly longer. The difference between inductive and non-inductive is a maximum at $t_1=0$, where it takes the non-inductive cases $0.8\ t_0$ for the current to build up in response to an instantaneous application of the full current-drive source.

During the transient phase, it is interesting to compare how distorted the plasma current profile becomes as it approaches steady state. To this end, we plot in Fig. 9 the minimum values of the plasma internal inductance, $l_i/2$ and of the plasma current peakedness, q^*/q_0, as a function of the current turnon time t_1 for the inductive rampup as well as for the non-inductive CD rampup with 0%, 50%, and 90% bootstrap current fraction. Another perspective on these trajectories can be obtained from Fig. 10 where we plot the trajectories in ($l_i/2$, q^*/q_0) space as time progresses from the initial application of the current drive to the attainment of steady state. This parameter space was introduced in [15] as a stability diagram for low-β plasmas. Upon comparison with the Fig. 4 of that paper, we see that the inductive trajectories of Fig. 10(a) remain in the stable regime even for $t_1 = 0.1\ t_0$, while the non-inductive bootstrap trajectories of Figs. 10(b) and 10(c) enter far into the unstable regimes for $t_1 < t_0$.

The results of the 1D calculations presented in Figs. 7 through 10 can be better understood by considering Eqs. (8), (13), (15), and (16), and the associated graph in Fig. 11. The source term $j_{CD}(r,t)$ as defined in Eq. (13) is manifestly positive and well behaved, as seen from its graph in Fig. 11(a). When inserted into Eq. (8), it will act to everywhere decrease ψ, as is needed to increase the plasma current non-inductively.

However, if we consider the evolution equation for the current density, Eqs. (15) and (16), obtained by twice differentiating Eq. (8), the picture is quite different. The source term $S_{CD}(r,t)$ in these equations and graphed in Fig. 11 is not as well behaved. It changes sign as a function of r and it becomes large and negative near the origin, actually diverging at $r \rightarrow 0$ for $f_{BS} > 0$. Thus, while the current density will eventually increase everywhere, we see that for short times it will first decrease at some locations, particularly near the plasma center.

V. Discussion

We can infer the relevant timescales from Eq. (15) even without solving it explicitly. The homogeneous part of this equation is the same as that analyzed in [13] with the "free current decay" boundary condition in that paper corresponding to our "non-inductive" boundary condition and the "constant plasma current" boundary condition corresponding to our "inductive" boundary condition. Since the value of ψ needs to change most on axis when going from the initial to the final state, it is clear that the n=1 eigenmode is the most relevant. That paper observed that the time constant for the n=1 mode for the "free current decay" was about 5-6 times longer than the corresponding time constant for the "constant plasma current" mode. This is consistent with what we found in our numerical experiments.

Also, Ref. [13] did not consider explicit source terms in the diffusion equation. The fact that these source terms peak near the magnetic axis (r=0) when bootstrap current drive is present, ie. Fig. 11(c), implies that there will be additional weighting to the value of the plasma resistivity near the origin. Thus, it is clear that the relevant timescale over which the current can be increased by non-inductive means without substantially distorting the shape of the current profile is given by

$$\tau = a^2 \mu_0 / \eta(0)\ f_P \qquad (19)$$

Where $\eta(0)$ is the central value of the resistivity and f_P is a profile-dependent factor very close to one, $f_P \approx 1$.

VI. Relation to Experiment

There are experimental results of RF being used to increase the plasma current in a toroidal device on WT-2 [16], TII-U [17], PLT [18-19], Alcator-C[20], and CDX-U [21-22]. The results of the first five of these are summarized in Table 2, while those in CDX-U are more difficult to interpret for the reasons stated below. Note that in Table 2, the first row of data is the central skin time based on the central electron temperature and the quoted Z_{EFF} , the second row is the incremental increase in the plasma current via non-inductive current drive, and the final row is the ratio of the current rampup time to the central skin time. The fact that T / τ_0 is greater than or comparable to $\Delta I / I$ in all these experiments is consistent with the results of our paper.

Table II: Summary of non-inductive current rampup experiments

	WT-2[16]	T-IIU [17]	PLT[18]	PLT [19]	Alcator-C[20]
$\tau_0 = a^2\mu_0/\eta(0)$	0.2 ms	5.8 ms	0.3 s	1.65 s	0.42 s
$\Delta I / I$	4	8	3.3	0.18	0.4
T / τ_0	105	27	7.6	0.18	0.35

The results of Table II also appear to be consistent with detailed simulations using TSC. For example, our simulations of the PLT current drive experiments reproduce the experimental results presented in Fig. 1 of [19] when the parameters quoted there are used. Namely for a = 0.3 m and R = 0.8 m, we considered the plasma response to shorting the OH supply while the equivalent of 300 kA of RF current drive is applied to increase the current of a 190 kA plasma with central T_e = 1.35 keV and Z_{EFF} = 4. Applying this current drive source in a period of 0.3 seconds resulted in a plasma current of 225 kA at the end of that period. The remaining 75 kA can be considered to be “back current”, consistent with the analysis in that paper.

The only experimental reference of possible bootstrap-overdrive plasma current buildup is in CDX-U [21-22]. There it is reported that the plasma bootstrap current was largely responsible for increasing the current of an a=0.2 m , T_e = 30 eV plasma from 600 A to 1000 A in 10 ms. These times also appear to be consistent with the analysis presented here, however, it is difficult to make direct comparison with this experiment without modeling the current due to the precessing orbits of the mirror confined plasma, including that on the open field lines.

VII. Summary and Conclusions

Plasma current rampup in an axisymmetric toroidal device is fundamentally different for *non-inductive* current drive than it is for *inductive* current drive. The first involves decreasing the total poloidal magnetic flux in the plasma center, while the second involves increasing this flux at the plasma edge.

Inductive current drive for a low-aspect-ratio axisymmetric toroidal device requires an OH solenoid at the small major radius side of the plasma, threading the torus. The "vertical field" produced by outer ring coils alone can never provide the flux needed to increase the plasma current.

We have shown by simulation that it should be possible to increase the plasma current in a low-aspect-ratio toroidal device using primarily the bootstrap effect, with only 10% or less of the driven current provided by external current drive, such as RF. However, the time required to increase the current is very long, and the maximum final plasma current will be proportional to the maximum possible toroidal field strength of the device.

The natural non-inductive current rampup time for a toroidal device scales similar to the inductive rampup time, but is set by the central resistivity and is therefor much longer, at least by a factor of 4-5 for the same temperature plasma. For a plasma with minor radius a and central resistivity $\eta(0)$, the natural non-inductive time is approximately given by

$$T = \mu_0 a^2 / \eta(0) \quad .$$

The long time required for current rampup is also compounded because the current drive systems and auxiliary heating systems needed to provide the plasma pressure for the bootstrap current also increase the plasma temperature and hence decrease the central resistivity and lengthen the natural time scales.

If current drive is applied over times much shorter than this natural time, unstable transients will dominate. The transients are more severe the higher the bootstrap fraction. However, if the heating and current drive sources are applied over times comparable to or longer than the “natural time”, i.e. $t \geq T$, then transients should not be a problem.

VIII. Acknowledgements

The author is grateful to Dr. M. Peng for calling attention to the importance of this problem, and to Drs. N. Pomphrey, D. Moreau, P. Politzer, F. W. Perkins and C. Kessel for useful discussions. This work was supported by DoE contract # DE-AC02-76-CHO-3073.

References:

[1] Y. K. M. Peng and D. J. Strickler, “Features of Spherical Torus Plasmas”, Nuclear Fusion **26** (1986) 769

[2] A. Sykes, G. Cunningham, R. Colchin, et al, “First results from the START experiment”, Nuclear Fusion **32** 695 (1992)

[3] A. Sykes, et al., “Mega-Ampere Spherical Torus Experiment”, United Kingdom Atomic Energy Authority, Culham Laboratory, England

[4] R. Fonk, T. Thorson, and the PEGASUS Team, “Plasma Behavior in the PEGASUS Toroidal Experiment”, Bull. Am. Phys. Soc. [RP1.37] (1999)

[5] M. Ono, S. Kaye, M. Peng, et al, “Exploration of Spherical Torus Physics in the NSTX Device”, IAEA-CN-69/ICP/01(R)-EX4/1(R), 17th IAEA Fusion Energy Conference Yokohama, Japan, 19-24 October 1998.

[6] S. C. Jardin, C. E. Kessel, J. Menard, et al, “Physics Basis for a Spherical Torus Power Plant”, submitted to Fus. Eng. Design (1999)

[7] N. Fisch, “Theory of Current Drive in Plasmas”, Rev. Mod. Phys. **59** 175 (1987)

[8] B. A. Nelson, T.R.Jarboe, D.J.Orvis, et al, “Formation and Sustainment of a 150 kA Tokamak by Coaxial Helicity Injection”, Phys. Rev. Lett. **72** (1994) 3666

[9] S. C. Jardin, N. Pomphrey, and J. DeLucia, “Dynamic Modeling of Transport and Positional Control of Tokamaks”, J. Comput. Phys. **66** (1986) 481

[10] S. C. Jardin, M. Bell , N. Pomphrey, “TSC Simulation of Ohmic Discharges in TFTR”, Nucl. Fusion **33** (1993) 317

[11] J. Greene, J.L. Johnson, and K. Weimer, “Tokamak Equilibrium”, Phys. Fluids **14** 671 (1971)

[12] M. Kruskal and R. Kuslrud, “Equilibrium of a Magnetically Confined Plasma in a Toroid”, Phys. Fluids **1** (1958) 265

[13] D. R. Mikkelsen, “Current Relaxation time scales in toroidal plasmas”, Phys. Fluids B **1**, p. 333 (1989)

[14] S. P. Hirshman and G. H. Neilson, “External Inductance of an Axisymmetric Plasma”, Phys. Fluids 29 (1986) 790

[15] C. Z. Cheng, H. P. Furth and A. H. Boozer, “MHD Stable Regime of the Tokamak”, Plasma Physics and Controlled Fusion, **29**, p. 351 (1987)

[16] S. Kubo, M. Nakamura, T. Cho, et al, “Toroidal Plasma Current Startup and Sustainment by rf in the WT-2 Tokamak”, Phys. Rev. Lett., **50**, p. 1994 (1983)

[17] K. Toi, K. Ohkubo, K. Kawahata, et al, “Startup and Quasistationary Drive of Plasma Current by Lower Hybrid in a Tokamak”, Phys. Rev. Lett.,**52**, p. 2144 (1984)

[18] F. Jobes, J. Stevens, R. Bell, S. Bernabei, A. Cavallo, et al, “Formation of a 100-kA Tokamak Discharge in the Princeton Large Torus by Lower Hybrid Waves”, Phys. Rev. Lett., **52**, p. 1005 (1984)

[19] F. C. Jobes, S. Bernabei, T. K. Chu, W. M. Hooke, E. B. Meservey, R. W. Motley, J. E. Stevens, and S. von Goeler, “Current Rampup by Lower-Hybrid Waves in the PLT Tokamak”, Phys. Rev. Lett., **55**, p. 1295 (1985)

[20] Y. Takese, S. Knowlton, and M. Porkolab, “Plasma current ramp-up and Ohmic-heating transformer recharging experiments using lower-hybrid waves on a tokamak”, Phys. Fluids **30**, p 1169 (1987)

[21] C. B. Forest, Y.S. Hwang, M. Ono, and D. Darrow, “Internally Generated Currents in a Small-Aspect-Ratio Tokamak Geometry”, Phys. Rev. Lett., **68** 3559 (1992)

[22] Y. S. Hwang, C.B. Forest, M.Ono, “Observation of Nonclassical Radial Current Diffusion in a Fully bootstrap Current Driven Tokamak”, Phys. Rev. Lett., **77**, 3811 (1996)

[23] F. Kazarian-Vibert, X. Litaudon, D. Moreau, et al, “Full steady-state operation in Tore Supra”, **38** p. 2113 (1996)

[24] C. Litwin, “Current Diffusion and Toroidal Electric Field Response to a non-Ohmic Current Drive”, Phys. Plasmas **2**, p. 4542, 1995

Figure Captions:

1. Basic geometry is shown. (R,φ,Z) form a standard cylindrical coordinate system. An OH coil, if present, has radius R_{OH} and height d. The poloidal angle about the magnetic axis is θ.

2. Poloidal magnet flux as a function of major radius for several times during plasma current buildup for (a) inductive buildup and (b) non-inductive buildup. Open triangles correspond to the magnetic axis and solid dots to the plasma boundary, or limiter.

3. Time histories of plasma parameters for the high-bootstrap non-inductive current buildup (a) toroidal current, (b) vacuum toroidal field, (c) poloidal flux, (d) poloidal beta and internal inductance, (e) safety factor, and (f) toroidal beta based on vacuum field and Troyon coefficient.

4. Plasma pressure vs. major radius on midplane for the high-bootstrap non-inductive current buildup.

5. Toroidal current density vs. major radius on midplane for the high-bootstrap non-inductive current buildup.

6. Toroidal current density (left) and poloidal flux (right) at t=140 s for the high-bootstrap non-inductive current buildup.

7.Time history of plasma current and internal inductance for a current rampup in time 0.1 t_0 for (a) inductive current rampup, (b) non-inductive current drive with 50% bootstrap current, and (c) non-inductive current drive with 90% bootstrap current.

8. Dependence of plasma current buildup time on CD source turnon time.

9. Dependence of (a) minimum internal inductance and (b) minimum current peakedness on CD source turnon time.

10. Trajectory in stability space for (a) inductive current rampup with a transformer, (b) current drive rampup with 50% bootstrap current, and (c) current drive rampup with 90% bootstrap current.

11. Profiles of (a) current drive source in flux evolution equation, (b) current drive source multiplied by plasma resistivity, and (c) current drive source in current evolution equation.

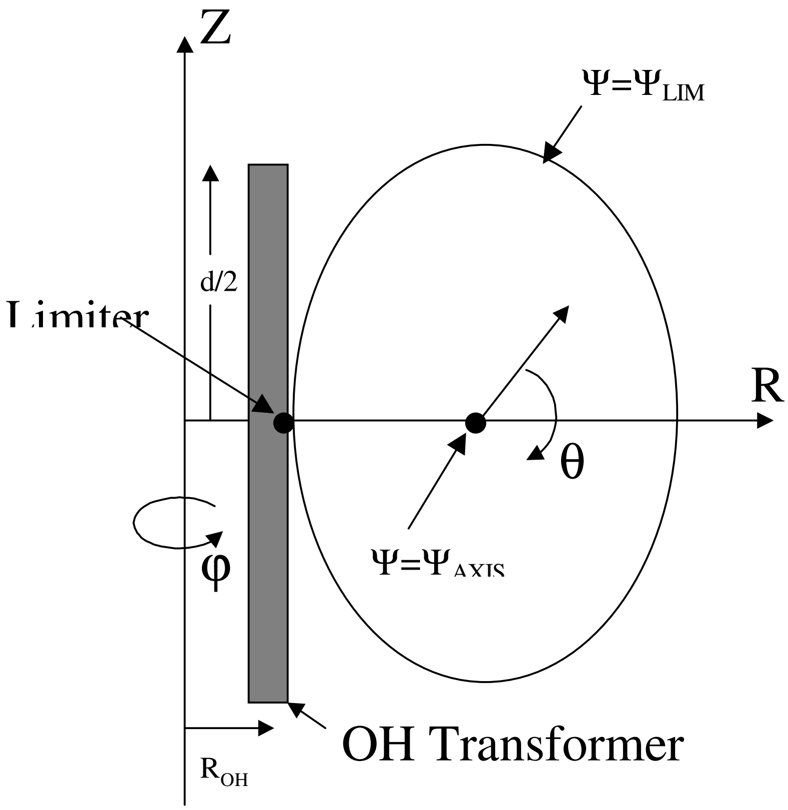

Figure 1: Basic geometry is shown. *(R,φ,Z)* form a standard cylindrical coordinate system. An OH coil, if present, has radius R_{OH} and height d. The poloidal angle about the magnetic axis is θ.

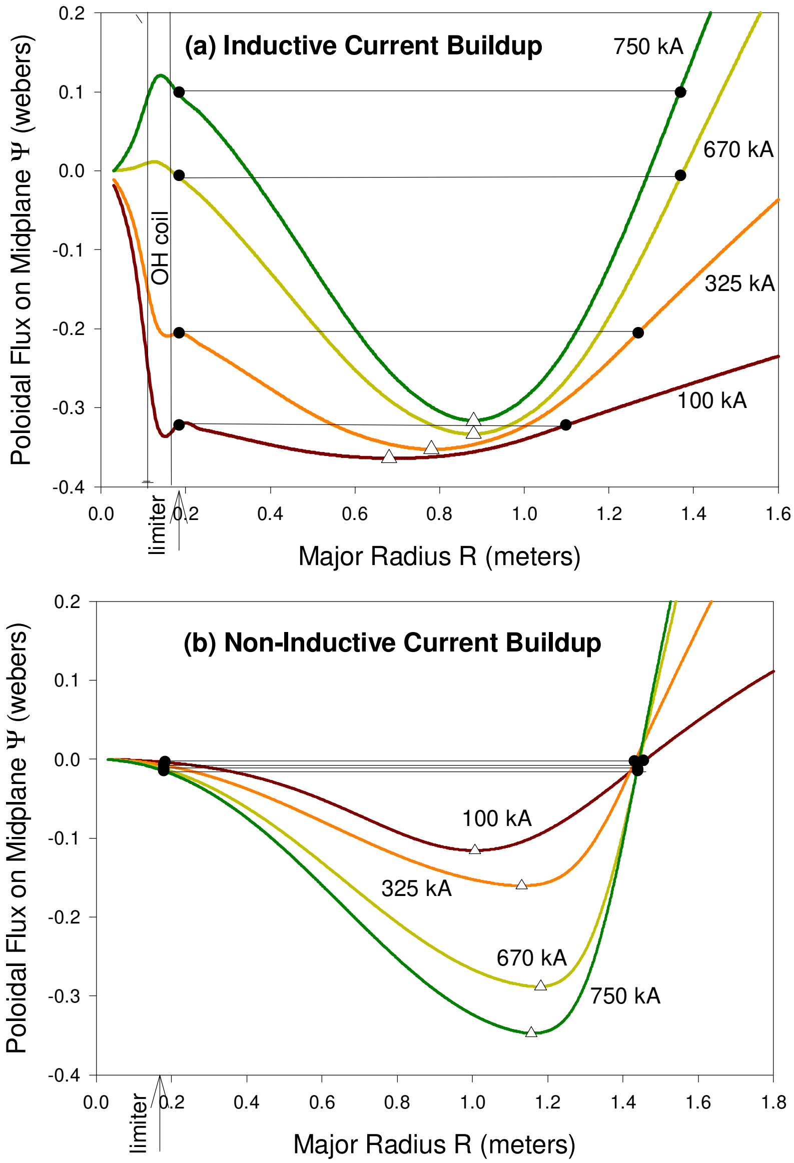

Figure 2: Poloidal magnet flux as a function of major radius for several times during plasma current buildup for (a) inductive buildup and (b) non-inductive buildup. Open triangles correspond to the magnetic axis and solid dots to the plasma boundary, or limiter.

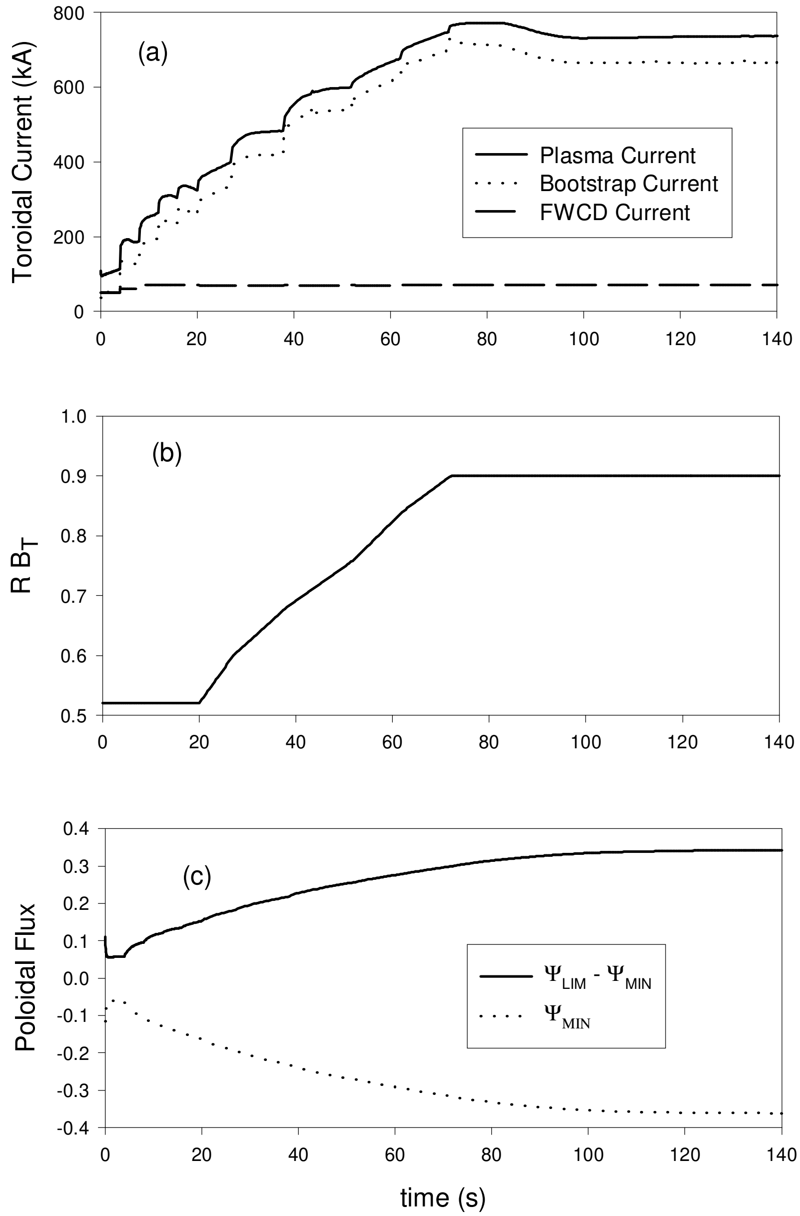

Figure 3: Time histories of plasma parameters for the high-bootstrap non-inductive current buildup (a) toroidal current, (b) vacuum toroidal field, (c) poloidal flux,

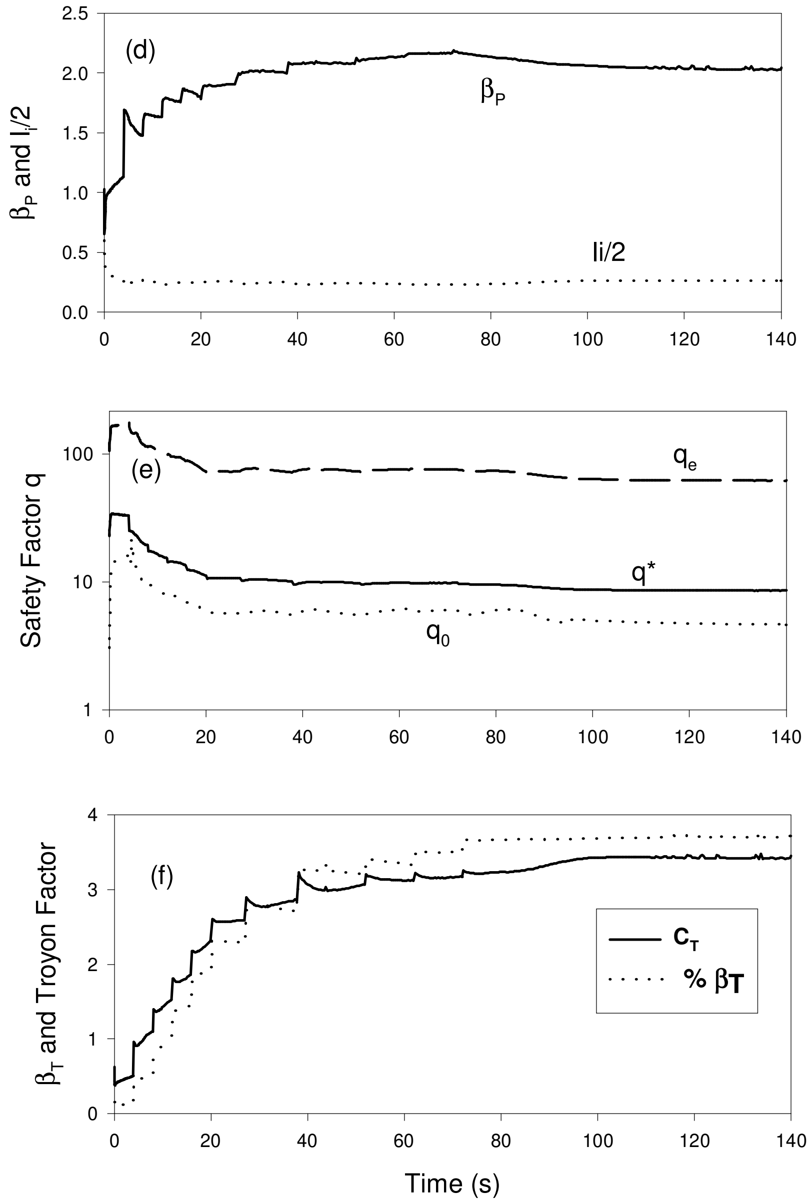

Figure 3: (d) poloidal beta and internal inductance, (e) safety factor, and (f) toroidal beta based on vacuum field and Troyon coefficient.

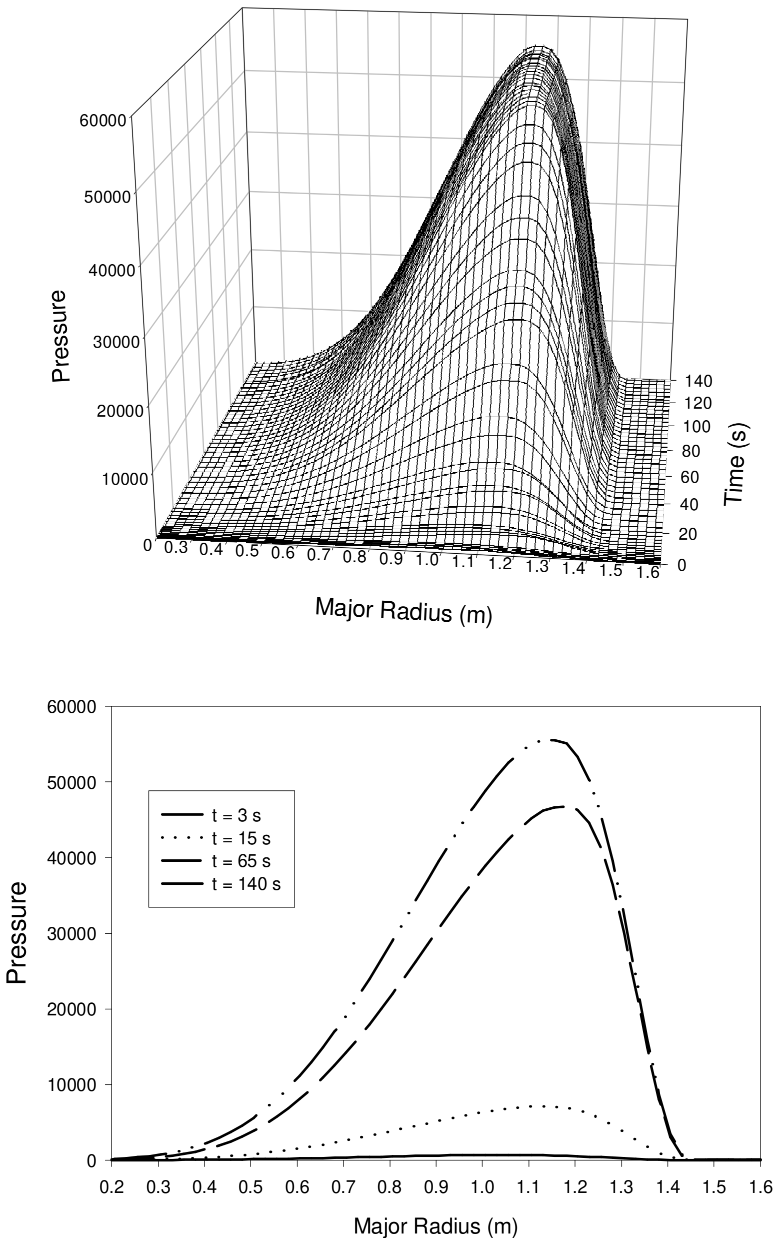

Figure 4: Plasma pressure vs. major radius on midplane for the high-bootstrap non-inductive current buildup.

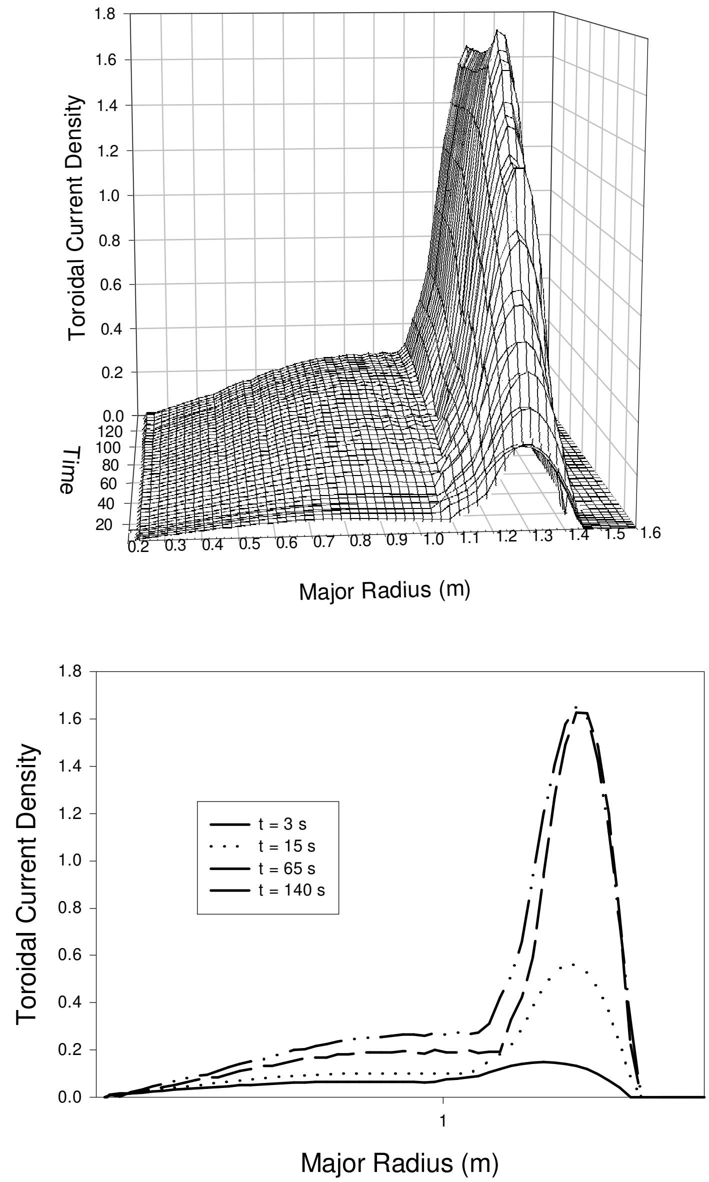

Figure 5: Toroidal current density vs. major radius on midplane for the high-bootstrap non-inductive current buildup.

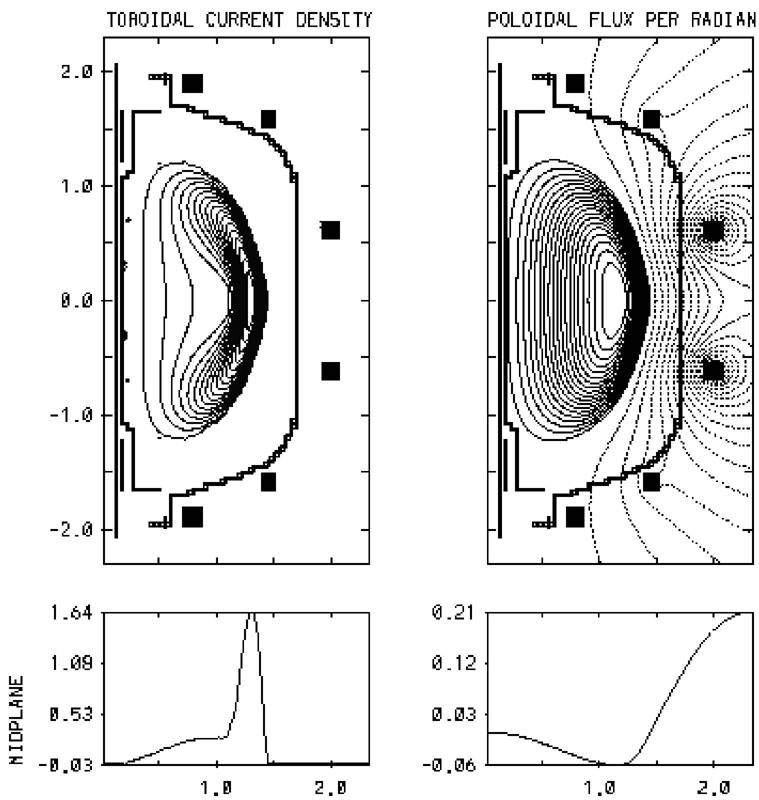

Figure 6: Toroidal current density (left) and poloidal flux (right) at t=140 s for the high-bootstrap non-inductive current buildup.

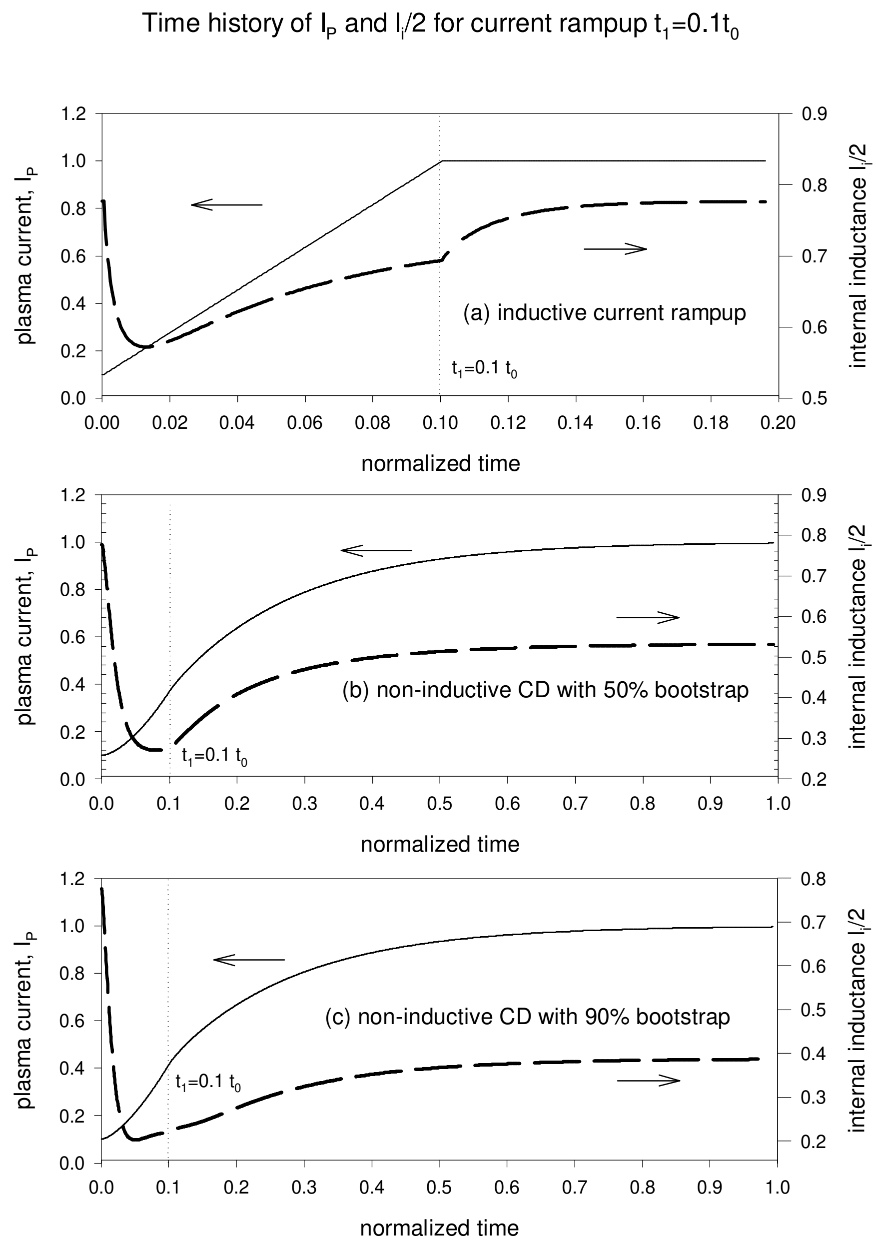

Figure 7: Time history of plasma current and internal inductance for a current rampup in time 0.1 t_0 for (a) inductive current rampup, (b) non-inductive current drive with 50% bootstrap current, and (c) non-inductive current drive with 90% bootstrap current.

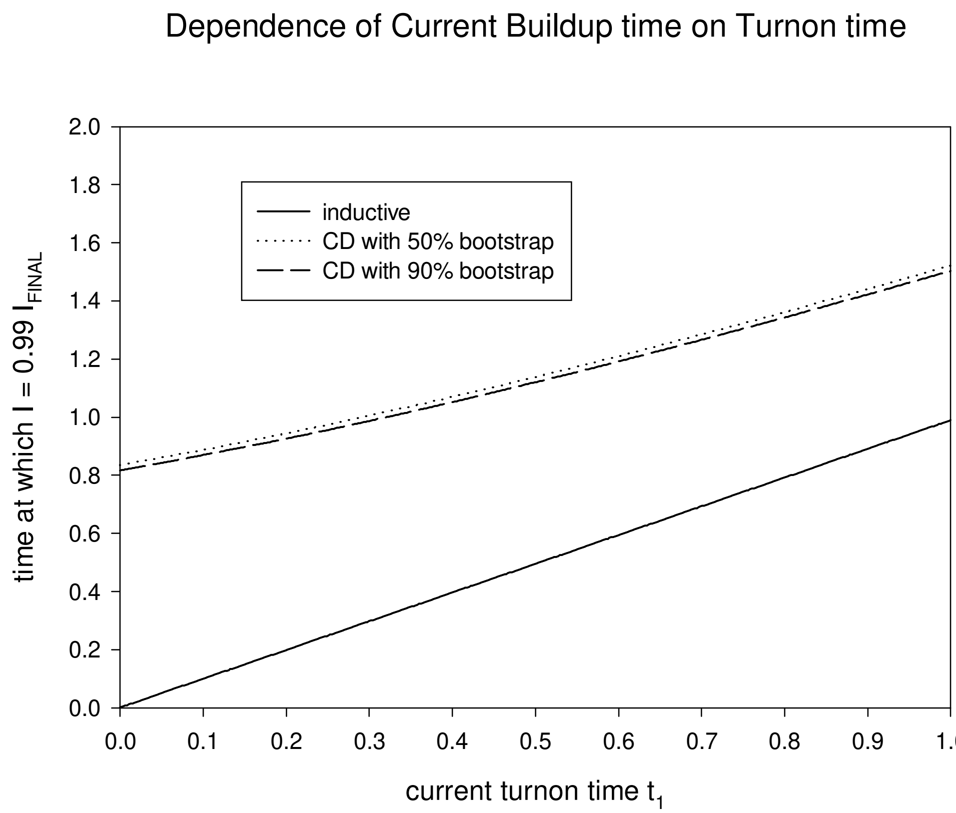

Figure 8: Dependence of plasma current buildup time on CD source turnon time

Dependence of minimum internal inductance on turnon time

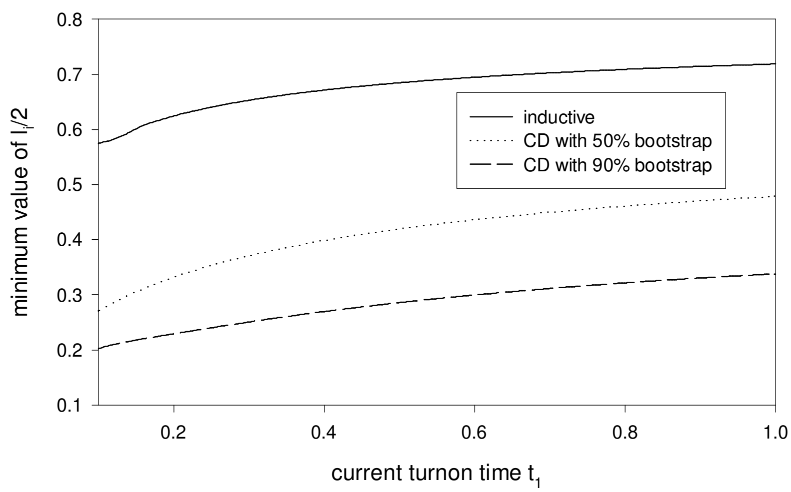

Dependence of minimum current peakedness on turnon time

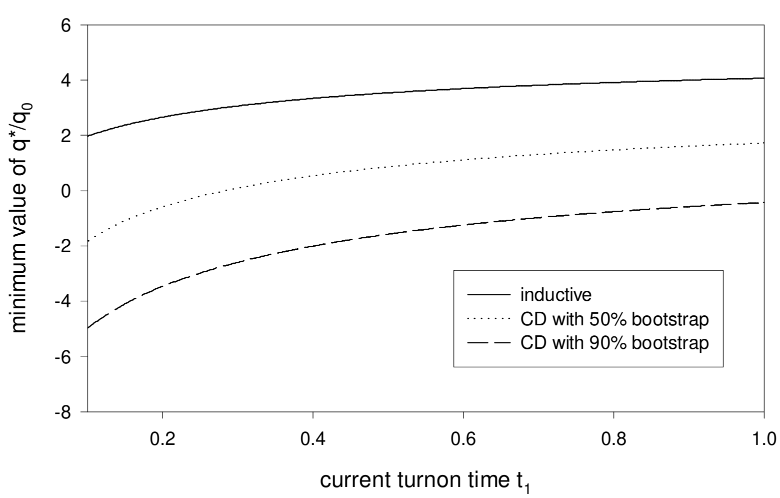

Figure 9: Dependence of (a) minimum internal inductance and (b) minimum current peakedness on CD source turnon time.

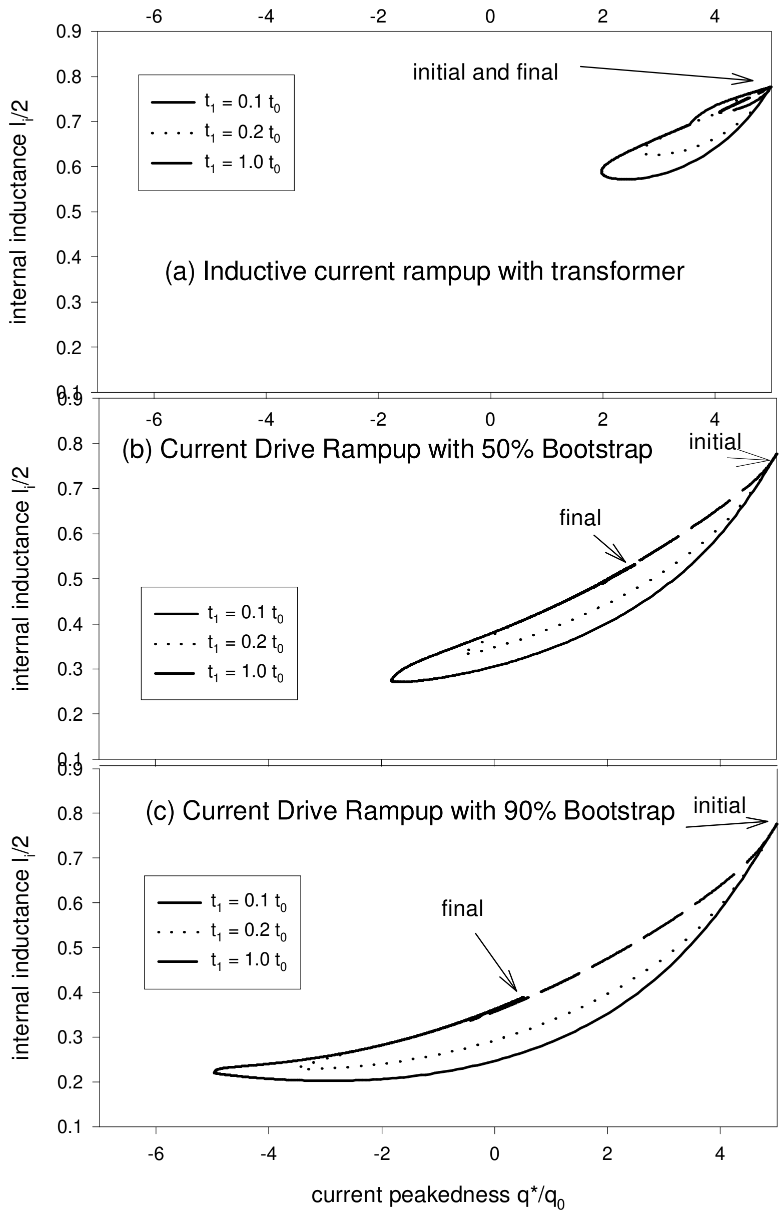

Figure 10: Trajectory in stability space for (a) inductive current rampup with a transformer, (b) current drive rampup with 50% bootstrap current, and (c) current drive rampup with 90% bootstrap current.

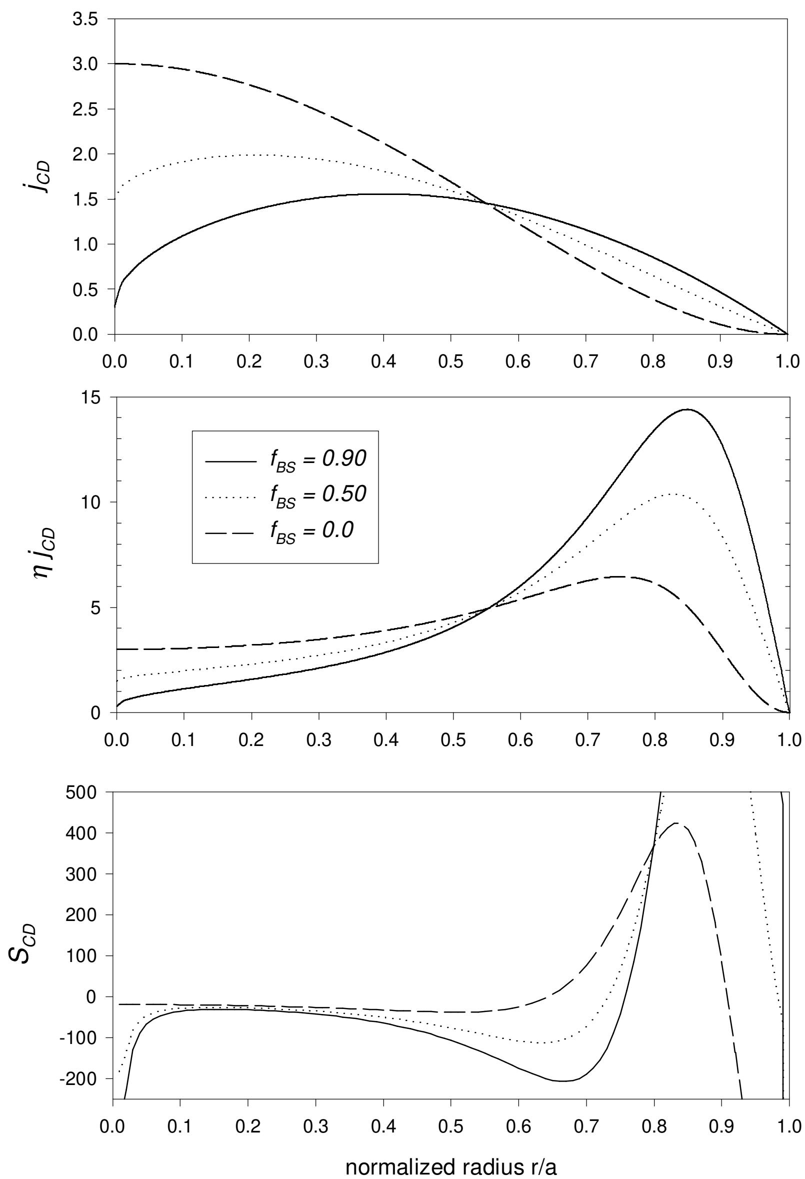

Figure 11: Profiles of (a) current drive source in flux evolution equation, (b) current drive source multiplied by plasma resistivity, and (c) current drive source in current evolution equation.